Physical mixing in coastal waters controls and decouples nitrification via biomass dilution

Sebastian Haas[a,1], Brent M. Robicheau[b], Subhadeep Rakshit[a], Jennifer Tolman[b], Christopher K. Algar[a], Julie LaRoche[b], and Douglas W. R. Wallace[a,1]

[a]Department of Oceanography, Dalhousie University, Halifax, NS, B3H 4R2, Canada; and [b]Department of Biology, Dalhousie University, Halifax, NS, B3H 4R2, Canada

Edited by Donald E. Canfield, University of Southern Denmark, Odense M, Denmark, and approved March 18, 2021 (received for review March 23, 2020)

Nitrification is a central process of the aquatic nitrogen cycle that controls the supply of nitrate used in other key processes, such as phytoplankton growth and denitrification. Through time series observation and modeling of a seasonally stratified, eutrophic coastal basin, we demonstrate that physical dilution of nitrifying microorganisms by water column mixing can delay and decouple nitrification. The findings are based on a 4-y, weekly time series in the subsurface water of Bedford Basin, Nova Scotia, Canada, that included measurement of functional (*amoA*) and phylogenetic (16S rRNA) marker genes. In years with colder winters, more intense winter mixing resulted in strong dilution of resident nitrifiers in subsurface water, delaying nitrification for weeks to months despite availability of ammonium and oxygen. Delayed regrowth of nitrifiers also led to transient accumulation of nitrite (3 to 8 μmol · kg_{sw}^{-1}) due to decoupling of ammonia and nitrite oxidation. Nitrite accumulation was enhanced by ammonia-oxidizing bacteria (*Nitrosomonadaceae*) with fast enzyme kinetics, which temporarily outcompeted the ammonia-oxidizing archaea (*Nitrosopumilus*) that dominated under more stable conditions. The study reveals how physical mixing can drive seasonal and interannual variations in nitrification through control of microbial biomass and diversity. Variable, mixing-induced effects on functionally specialized microbial communities are likely relevant to biogeochemical transformation rates in other seasonally stratified water columns. The detailed study reveals a complex mechanism through which weather and climate variability impacts nitrogen speciation, with implications for coastal ecosystem productivity. It also emphasizes the value of high-frequency, multiparameter time series for identifying complex controls of biogeochemical processes in aquatic systems.

nitrifier diversity | Thaumarchaeota | nitrite accumulation | time series | aquatic nitrogen biogeochemistry

Coastal waters worldwide are subject to inputs of anthropogenic nitrogen (N) which impact primary production and marine ecosystems through alteration of both the quantity and speciation (oxidized/reduced and inorganic/organic) of N (1, 2). These are key controls on phytoplankton growth and community composition, altering patterns and magnitude of primary production, causing eutrophication and harmful algae blooms and impacting carbon flux (2–4). For example, relative increase in ammonium over nitrate supply can shift phytoplankton community compositions toward smaller species with the potential to cause harmful algal blooms and reduced productivity (2). The speciation of N also exerts control on key microbial N cycling pathways, including the fixed N removal processes anammox and denitrification. These pathways depend on the availability of oxidized forms of N that can be converted to N_2 and thereby removed from the pool of readily bioavailable N within ocean waters.

It is therefore essential to understand the processes and environmental factors that control the speciation of dissolved inorganic nitrogen (DIN = NO_3^- + NO_2^- + NH_3/NH_4^+) between oxidized (nitrate and nitrite) and reduced (ammonium/ammonia) forms as well as between organic and inorganic forms (2, 5). A central process controlling DIN speciation is nitrification, the two-step oxidation of ammonia (NH_3) to nitrate (NO_3^-) via nitrite (NO_2^-). Ammonia-oxidizing organisms (AOO), either archaea (AOA) from the phylum *Thaumarchaeota* or bacteria (AOB), catalyze the oxidation of ammonia to nitrite:

$$\text{Ammonia oxidation (AO):}\quad 2NH_3 + 3O_2 \rightarrow 2NO_2^- + 2H^+ + 2H_2O. \qquad [1]$$

AO kinetics differ between the two AOO groups, with higher maximum reaction velocities (V_{max}) and ammonium half-saturation constants (K_m) in AOB (6–8) compared to AOA (9–11). Nitrite-oxidizing bacteria (NOB) are responsible for the second step from nitrite to nitrate:

$$\text{Nitrite oxidation (NO):}\quad 2NO_2^- + O_2 \rightarrow 2NO_3^-. \qquad [2]$$

Recently, an exception to the two-organism nitrification paradigm (12, 13) has been recognized through the discovery of complete ammonia oxidation to nitrate ("comammox") by individual *Nitrospirae* bacteria (12, 13). This could play a role in coastal marine waters under some conditions (14).

Significance

Changes in both quantity and speciation of nitrogen in coastal waters impact phytoplankton communities, contributing to eutrophication and harmful algal blooms. Multidisciplinary oceanographic time series of high resolution are rare but crucial for identifying complex mechanisms that underlie such anthropogenic impacts. Analysis and modeling of such a time series from a seasonally stratified fjord showed that dilution of nitrifier biomass by variable winter mixing altered the timing and rates of nitrification, which converts ammonia to nitrite and nitrate. This reveals a link among climate-sensitive physical dynamics, nitrifier abundance, and diversity, with controls on phytoplankton ecology. The findings imply that explicit measurement and modeling of microbial communities will be required to project impacts of climate change on coastal ecosystems.

Author contributions: S.H., J.L., and D.W.R.W. designed research; S.H., B.M.R., S.R., and J.T. performed research; B.M.R. and J.T. designed quantitative molecular assays; S.H., B.M.R., and S.R. analyzed data; S.H., B.M.R., and S.R. wrote the paper; S.R. and C.K.A. created and developed numerical models; and C.K.A., J.L., and D.W.R.W. advised during research, data analysis, and writing.

The authors declare no competing interest.

This article is a PNAS Direct Submission.

[1]To whom correspondence may be addressed. Email: s.haas@dal.ca or douglas.wallace@dal.ca.

This article contains supporting information online at https://www.pnas.org/lookup/suppl/doi:10.1073/pnas.2004877118/-/DCSupplemental.

Published April 26, 2021.

In the ocean, nitrification maxima typically occur at or below the base of the euphotic zone, spatially separated from photosynthetic primary production (10, 11, 15). However, vertical transport can supply products of nitrification to the euphotic zone (16, 17). Incomplete nitrification may therefore affect phototrophic communities, since the speciation of externally supplied N (e.g., ammonium versus nitrate) can significantly impact both the structure and productivity of phytoplankton (2).

Accumulation of the intermediate product of nitrification, nitrite, has been documented in a wide range of marine systems, including at the base of the oceanic euphotic zone (18) and transiently in coastal bights, bays, and estuaries (19–23). In many cases, the presence of nitrite can be attributed to decoupling of AO and NO, which are usually tightly coupled despite ecophysiological differences between AOA and NOB (24). A large variety of environmental factors, including temperature and oxygen, have been associated with the decoupling of nitrification in marine systems (19, 20, 25, 26). Here, we describe nitrite accumulation arising from nitrifier regrowth following physical dilution, which might point to a role for nitrifier biomass in a more general mechanism for decoupling nitrification in seasonally stratified water columns.

Physical transport is widely recognized to control phytoplankton growth in aquatic systems, for example through supply of nutrients to the euphotic zone from below (17, 27). Mixing also plays a role in the initiation of spring blooms according to the "dilution-recoupling" hypothesis (28), which posits that dilution of both phytoplankton and grazer biomass leads to fewer grazer–phytoplankton encounters. It has been shown that nitrification can be enhanced by the mixing of ammonium-rich waters into well-oxygenated waters (21, 29), whereas the mixing-induced transport of NOB biomass away from the depth of optimal growth at the base of the euphotic zone has recently been implicated as a factor explaining local nitrite accumulation (30). Here, we describe a different way in which mixing controls nitrification, whereby seasonal and interannual variations in mixing lead to temporally variable rates of nitrification as a consequence of nitrifier biomass dilution.

High-frequency, long-term measurements of the physical and chemical environment along with the associated microorganisms have been shown to be a valuable tool set for determining environmental controls on microbial processes (17, 31–35). However, such time series are rare because of the sustained, multidisciplinary effort and teamwork they require.

Here, we present results of such a time series–based study of nitrification within the bottom water (60 m) of Bedford Basin (BB), a eutrophic, anthropogenically impacted, fjord-like embayment located within the Halifax Regional Municipality on the Atlantic coast of Nova Scotia, Canada (see *SI Appendix, SI Materials and Methods* for more details). Restricted water exchange with the open ocean and annual cycles of stratification and winter mixing make BB a useful natural laboratory to study the relationship between microbial growth phases, geochemistry, and physical processes. Based on 4 y of weekly observations of ammonia monooxygenase subunit A (*amoA*) gene copy numbers (via qPCR), microbial community composition (16S ribosomal RNA [rRNA] gene amplicon sequencing), nutrient concentrations, and a biogeochemical model enhanced by functional gene modeling, we observed variable dilution of the nitrifier population following winter mixing events. We propose that intense winter mixing during cold winters flushes the resident nitrifier population from the basin bottom waters, resulting in a delay in nitrification and decoupling of AO and NO until the nitrifier community can reestablish. During warmer winters, when mixing is less intense, growth can keep pace with mixing and effectively prevent dilution.

Study Setting and Time Series Context

The 4 y time series of molecular and chemical data from BB bottom water presented here (*SI Appendix, SI Materials and Methods*) was collected between January 2014 and December 2017, at the center of the basin (44°41′37″N, 63°38′25″W). Our study was conducted in the context of a longer, weekly oceanographic time series established in 1992 (32, 36). BB (70 m maximum depth) experiences annual cycles of turbulent winter mixing and seasonal stratification. Water above the sill depth (20 m) is subject to circulation and tidal exchange with the Atlantic Ocean (Scotian Shelf) throughout the year (37–39), while the bottom water is effectively disconnected from this circulation during stratified periods. Stratification is established in spring (approximately April) and persists into winter (November through February), when it breaks down due to intense cooling (36, 39). In some years, the stratified period is interrupted by the intrusion of relatively warm and saline water from the Scotian Shelf into the bottom water of the basin (31, 40, 41). Unlike the more extended periods of convective mixing during winter, these intrusions are short lived and do not break down the vertical stratification, but they do ventilate the bottom water and modify its biogeochemistry (31, 41). The fate of "older" bottom water that is displaced following an intrusion is not well characterized but presumably involves upwelling and mixing into near-surface layers followed by exchange with continental shelf-water. The euphotic zone (>1% surface irradiation) depth in BB is ≤25 m year-round so that the conditions in the bottom water (60 m) are permanently dark (36, 42).

AOA peptides and the presence of *Nitrospina*-type NOB have previously been detected in BB bottom water (43), which has a microbial community that is distinct from that in the near-surface waters (34). Despite continuous availability of ammonium (mostly >1 μmol · kg_{sw}^{-1}), AO rates are highly variable (31).

Results

Physical Mixing and Nutrient Cycling in BB, 2014 Through 2017. The mixing regime within BB between 2014 and 2017 displayed a sequence of full water column winter/spring mixing followed by stratification throughout summer and fall (Fig. 1) that was consistent with longer-term observations (*SI Appendix*, Fig. S1). During stratified periods, the bottom water was relatively isolated from near-surface water as indicated by consistently cold temperatures (~1 to 4 °C) despite strong near-surface temperature variability (~1 to 18 °C). Dissolved oxygen was an especially clear indicator of active mixing due to its nonconservative nature and near-surface source: periods of stratification were marked by a steady decline in bottom water oxygen and were clearly distinguishable from periods of mixing when oxygen was delivered to the bottom water (Fig. 2*A*).

The event markers M14, PM15, M16, and M17 in Fig. 2*A* show the end of winter mixing and onset of stratification each year around April as indicated by the beginning of steady oxygen decrease. The stratified periods were interrupted by occasional shelf water intrusions into the bottom water (Events I14, I16a, I16b, and I17, Figs. 1 and 2*A*). In July 2017, there was an intrusion of shelf water to mid-depth layers (~30 m) of BB (44). Some of this intruding water was entrained into the bottom layers during the subsequent weeks, as indicated by nitrate decrease and a transient delay in oxygen decrease at 60 m (Event MDI17, Fig. 2 *A* and *B*).

The intrusion events delivered warmer (0.5 to 2.3 °C temperature increase) and saltier (0.2 to 0.6 practical salinity units [PSU] increase) offshore water to the bottom of BB, whereas winter mixing decreased both the temperature and salinity of the bottom water (Fig. 1 *A* and *B*). The cooling and freshening effect of winter mixing and the contrasting effect of intrusions on BB bottom water are reflected in the "spiciness" of the water. Spiciness is a derived parameter that is proportional to both temperature and salinity and can be used to distinguish water types that share the same density (45). Sudden increases in spiciness occurred with each intrusion event (Events I14, I16a, I16b, and I17).

In contrast, rapid decreases in spiciness associated with winter mixing adding relatively cold and fresh water to the bottom layer

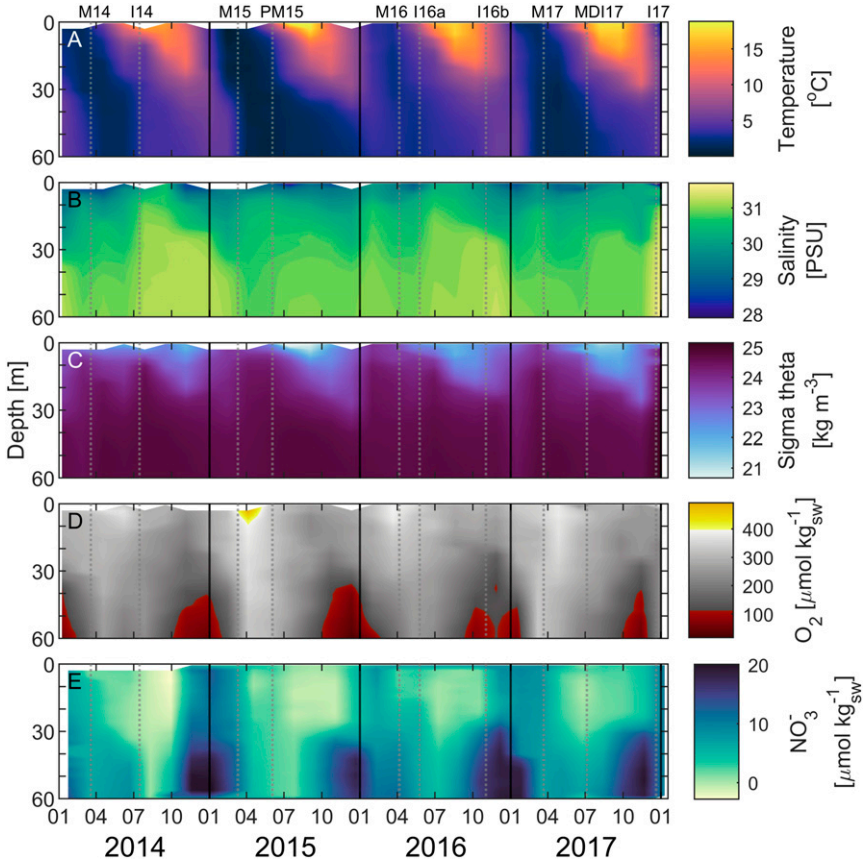

Fig. 1. Time series of weekly vertical profiles of temperature (*A*), salinity (*B*), sigma theta (potential density) (*C*), dissolved oxygen (*D*), and nitrate (*E*) in BB between January 2014 and December 2017. Event numbers indicate winter mixing ("M") or intrusion events ("I"). "MDI17" is an intrusion to middepth waters of BB. PM15 indicates the prolonged phase of winter mixing in 2015.

occurred in early 2014, 2015, and 2017 (Events M14, M15, and M17; Fig. 2*A*). They co-occurred with rapid increases in oxygen concentration, indicating intense winter mixing (Fig. 2*A*). The spiciness decrease in winter 2016 was much less pronounced (M16), whereas lowest spiciness was observed in late April 2015 (Fig. 2*A*), suggesting winter mixing was strongest in 2015 and weakest in 2016.

This is consistent with lower air temperatures during winter 2015 compared to winter 2016. Low temperatures drive winter mixing in BB through cooling of surface water (32, 39), and average January-through-March atmospheric temperatures recorded at Environment and Climate Change Canada's BB station were lowest in 2015 (−4.4 °C) and highest in 2016 (−0.5 °C), with intermediate values observed in 2014 (−2.7 °C) and 2017 (−1.6 °C). The average January-through-March temperatures since 2008, when data became available at this station, have been −1.5 °C (SD: 1.3 °C), and the winter temperatures in 2015 were the coldest on record for this station.

Additionally, higher values of buoyancy frequency (N^2, a measure of water parcel stability) in winter 2016 indicated stronger stratification than in other years (Fig. 2*A*). Taken together, these observations indicate that winter mixing was weakest in 2016 and strongest in 2015, whereas 2014 and 2017 represented intermediate cases.

Both winter mixing and intrusions led to increased dissolved oxygen and decreased DIN concentrations in the bottom water (Fig. 2 *A* and *B*). In all 4 y, ammonium concentrations increased with the onset of stratification (approximately April) due to remineralization of organic N, reaching maxima of 13 to 18 μmol · kg_{sw}^{-1} during the stratified period (Fig. 2*B*). The proportion of nitrate in DIN increased in late summer, indicating that nitrification exceeded the rate of N remineralization. Continuous water column profiles measured by a nitrate sensor (*SI Appendix, SI Materials and Methods*) showed that the vertical nitrate maximum in each year was located close to our standard sampling depth of 60 m (Fig. 1*E*). At the end of the stratified periods, ammonium typically decreased to relatively low concentrations ≤2.0 μmol · kg_{sw}^{-1}. However, in 2015, ammonium remained above ∼6 μmol · kg_{sw}^{-1} (Fig. 2*B*).

Despite these repeating patterns of physical mixing and ammonium accumulation, the timing of nitrate accumulation differed between years. The derivative of nitrate with respect to time (Fig. 3*D*), which can be used to assess the addition and removal of nitrate as a function of time, indicates that in 2016, nitrate began to increase immediately after the onset of stratification, whereas a delay in accumulation was observed following winter mixing in 2014 and 2015 (Fig. 2*B*).

Diversity of 16S rRNA Genes Affiliated with Nitrifiers. To examine the diversity of nitrifiers during the time series period, we analyzed the abundance of amplicon sequence variants (ASV) affiliated with the known nitrifiers *Thaumarchaeota* (AOA), *Nitrosomonadaceae* (AOB), and *Nitrospinaceae* (NOB). Relative abundances of nitrifier-affiliated ASVs were scaled to total microbial cell counts (Fig. 2 *C* and *D* and *SI Appendix, SI Materials and Methods*). The relative abundance of ASVs affiliated with nitrifiers (sum of *Thaumarchaeota*, *Nitrosomonadaceae*, and *Nitrospinaceae*) in the microbial community ranged from <0.1 to 38%, which corresponded to $2.1 \times 10^2 - 6.1 \times 10^5$ cells g_{sw}^{-1} after scaling to microbial cell counts (Fig. 2*C*). AOA abundance (max. 4.5×10^5 cells g_{sw}^{-1}) was similar to other coastal systems (33, 46).

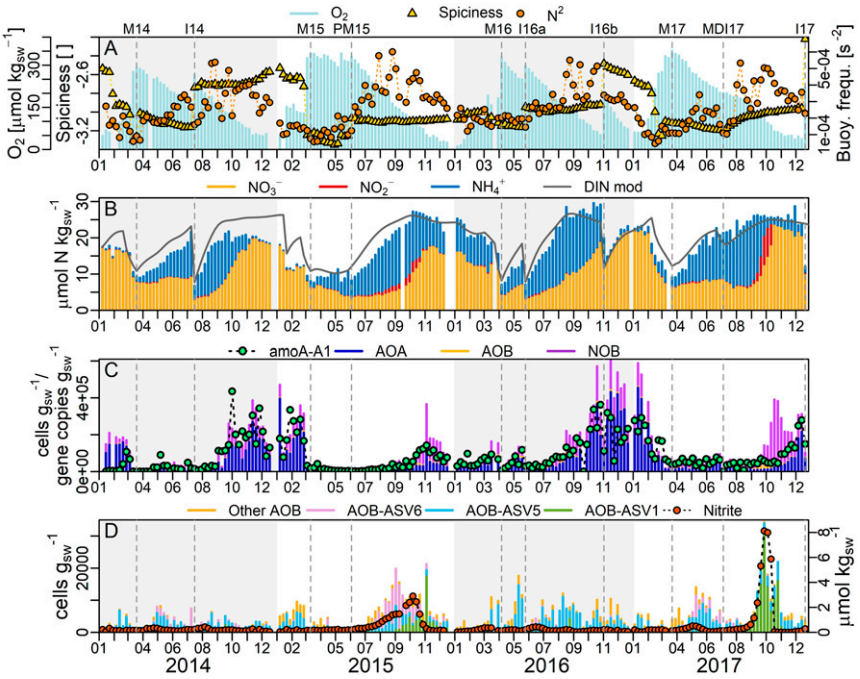

Fig. 2. Time series of biogeochemical parameters observed at 60 m in Bedford Basin, 2014 to 2017. (*A*) Buoyancy frequency (N^2), spiciness, and oxygen concentration. (*B*) Ammonium, nitrite, and nitrate concentration along with modeled DIN concentrations. (*C*) Abundance of Thaumarchaeota- (AOA), Nitrospinaceae- (NOB), and Nitrosomonadaceae (AOB)-affiliated ASVs, as well as amoA-A1. (*D*) Nitrite concentration and the abundance (based on percent total 16S rRNA amplicon sequences scaled to total cell counts) of ASVs affiliated with Nitrosomonadaceae (NOB). Event numbers ("M", "I", "PM", and "MDI") are as in Fig. 1.

The abundance of beta-AOB was low compared to AOA (Fig. 2*C*), but the larger cell sizes of AOB compared to AOA may entail higher biogeochemical impact per cell (9). The two most abundant *Thaumarchaeota*-affiliated ASVs in the BB bottom water, AOA-BB-ASV2 and AOA-BB-ASV3, were closely related and formed a distinct clade within the genus *Nitrosopumilus* (*SI Appendix*, Fig. S2*B*). AOA-BB-ASV3 was most abundant in 2015, while AOA-BB-ASV2 dominated in the remaining years.

AOB were affiliated with the betaproteobacterial family *Nitrosomonadaceae* (beta-AOB; *SI Appendix*, Fig. S2*A*). Beta-AOB-BB-ASV6, which formed a clade independent of the *Nitrosomonas* and *Nitrosospira* clades (bootstrap support >80%), showed a distinct maximum in fall 2015 (*SI Appendix*, Fig. S2 *A* and *D*). Beta-AOB-BB-ASV1, which fell into a cluster of *Nitrosomonas*-like BB sequences, had a maximum in fall 2017 and a smaller amplitude maximum in late fall 2015.

NOB were affiliated with the genus *Nitrospina* (*SI Appendix*, Fig. S2*A*). The three most abundant *Nitrospina*-affiliated ASVs showed minima in summer and maxima in fall/winter. *Nitrospirae*-affiliated 16S rRNA genes were present in only a few samples at very small percentage (<0.1%) and did not fall within the genus *Nitrospira* (*SI Appendix*, Fig. S2*A*), suggesting no role for comammox in BB bottom water during the study period (14).

Controls on the Temporal Distribution of *amoA* and Nitrifier-Affiliated 16S rRNA ASVs. To investigate how the timing of nitrification may be controlled by variations in nitrifier biomass and diversity, we further characterized the AOA by quantifying six marine phylotypes of the functional gene for ammonia oxidation, *amoA*. The most abundant archaeal phylotype was amoA-A1 (up to 4.4×10^5 *amoA* copies $\cdot$ g_{sw}^{-1}), which has been found primarily in ocean surface waters (47). Strong correlation between *Thaumarchaeota*-affiliated ASV and amoA-A1 abundance (Spearman's rho: $R^2 = 0.66$, $P < 1 \times 10^{-47}$; Fig. 2*C*) suggested that amoA-A1 variations tracked AOA abundance. The much lower abundance of the other phylotypes ($\leq 1.1 \times 10^4$ copies g_{sw}^{-1}) and their association with mixing events rather than nitrate concentration (*SI Appendix*, Fig. S3 and Table S1) suggest that these rarer phylotypes were transient populations, which were transported from near-surface or shelf waters but were unable to establish themselves in the bottom water of BB (*SI Appendix*, *SI Discussion S1*).

Only phylotype amoA-A1 correlated with nitrate (Spearman's rho: $R^2 = 0.42$; $P < 1 \times 10^{-24}$), and its abundance decreased during both winter mixing and intrusion events (Fig. 2*C*), which explains its inverse correlation with oxygen (Table 1 and *SI Appendix*, Fig. S4 and Table S1). This suggests that amoA-A1 was active and the dominant phylotype. However, in 2017, amoA-A1 abundance did not increase until after the period of rapid nitrite and nitrate increase (September/October; Fig. 2 *B* and *C*). A peak in the abundance of *Nitrosomonadaceae*-affiliated ASVs coinciding with this period of steep nitrite and nitrate increase in 2017 suggests a significant role for beta-AOB (Fig. 2 *B*–*D*).

A statistically significant correlation was identified between oxygen increases and decreases in the nitrifier proxies amoA-A1 as well as in the AOA and NOB cell densities (Table 1). This is suggestive of mixing-associated decreases that can be explained by dilution with BB near-surface water, which was depleted in AOA and NOB (*SI Appendix*, Fig. S5) and flushed by the near-surface estuarine circulation and tidal exchange with offshore waters (37–39). Thus, physical mixing with the near-surface water can act as a net sink for nitrifier biomass, diluting it within the bottom water. Winter mixing coincided with more pronounced nitrifier decreases than the intrusion events of 2014 and 2016 (I14, I16a, and I16b; Fig. 2*C*). The degree of amoA-A1 dilution within the bottom water due to winter mixing varied between years, with stronger amoA-A1 decrease in 2014 (minimum: 11 copies g_{sw}^{-1}, dilution factor $\sim 10^3$) and 2015 (min: 1.0×10^3 copies g_{sw}^{-1}, dilution factor $\sim 10^2$) compared to 2016 (5.6×10^3 copies g_{sw}^{-1}, dilution factor ~ 10) and 2017 (4.1×10^4 copies g_{sw}^{-1}, dilution factor ~ 10).

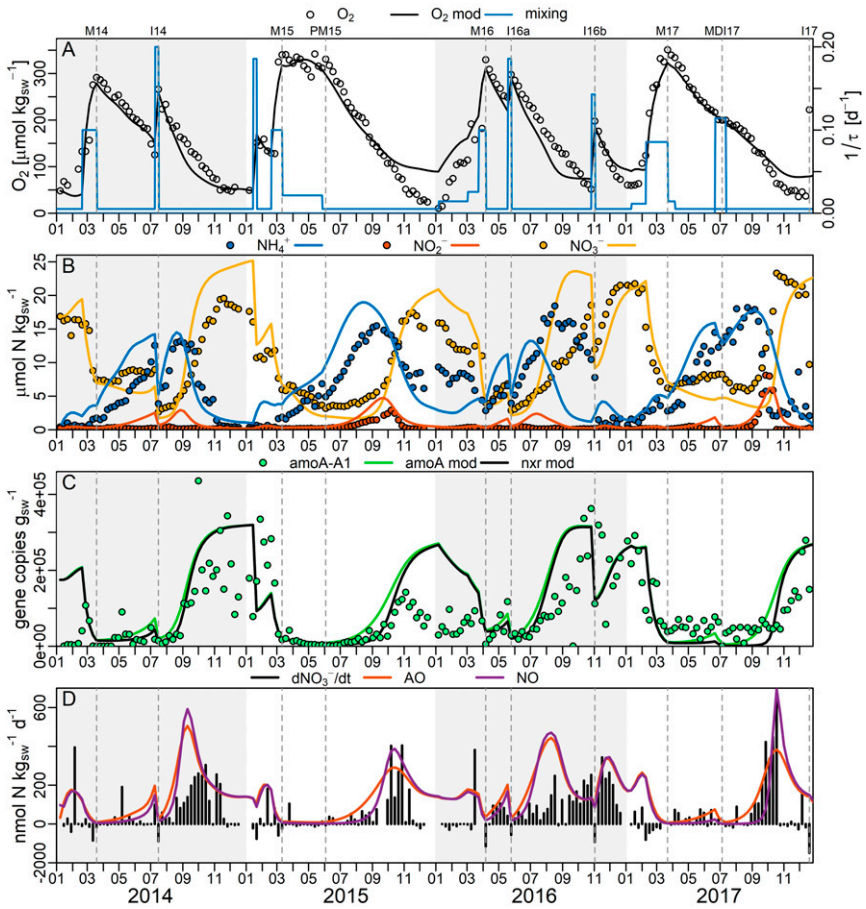

Fig. 3. Time series of observed (scatter or bar) and modeled (lines: "mod") biogeochemical parameters at 60 m in Bedford Basin, 2014 to 2017. (*A*) Oxygen concentrations (modeled and observed) and the inverse of residence time τ, describing the timescale of exchange of BB bottom water with water from the basin surface or the shelf. (*B*) Observed and modeled ammonium, nitrite, and nitrate concentrations. (*C*) AmoA-A1 (modeled and observed) and nxr (modeled) gene abundance. (*D*) Modeled rates of ammonia oxidation and nitrite oxidation as well as time derivative of observed nitrate concentration, dNO_3^-/dt (note the less detailed scale for negative values). Event numbers ("M", "I", "PM", and "MDI") as in Fig. 1.

After the strong dilution following winter mixing in 2014 and 2015 (Events M14 and M15, Fig. 2*C*), delayed regrowth of the nitrifier population was observed, which coincided with delayed nitrate accumulation during the same periods. Conversely, nitrate increased immediately following cessation of winter mixing in 2016 and 2017 (Events M16 and M17, Fig. 2*C*), when amoA-A1 winter-time minima were less pronounced. The increase in nitrate and amoA-A1 at the beginning of the 2017 stratified period was interrupted by the middepth intrusion of July 2017 (Event MDI17: Fig. 2*C*).

Table 1. Results from Spearman's Rho correlation tests between oxygen concentration, spiciness, nitrifier abundances, and their time derivatives (dx/dt) using 2014 to 2017 BB bottom water data

Parameter pair		n	r	p
O_2	amoA-A1	196	−0.59	3.9E−20
	AOA	197	−0.60	6.2E−21
	NOB	197	−0.76	6.2E−39
$d(O_2)/dt$	d(amoA-A1)/dt	188	−0.19	0.0105
	d(AOA)/dt	190	−0.28	0.0001
	d(NOB)/dt	190	−0.27	0.0002
d(spiciness)/dt	d(amoA-A1)/dt	193	−0.18	0.0106
	d(AOA)/dt	195	−0.27	0.0001
	d(NOB)/dt	195	−0.14	0.0460

A Biogeochemical Model of Nitrogen Cycling in BB Bottom Water. To gain mechanistic insight into the influence of winter mixing on nitrifier growth dynamics and nitrification rates, a simple N cycling box model was constructed for the BB bottom water (*SI Appendix*, Fig. S6 and Tables S2–S4). Conceptually, this model is analogous to a bioreactor, in which a resident population of nitrifiers actively grows below the pycnocline but can be diluted through time-varying exchange with BB near-surface water (by winter mixing) or Scotian Shelf water (by intrusions; *SI Appendix*, Fig. S6). During the stratified period, the nitrifiers remain relatively isolated from the near-surface water and dilution is negligible. During winter mixing or intrusion events, the population is subjected to dilution as the exchange term increases. If the dilution rate is much faster than the growth rate, then washout of the "bioreactor" can occur. At the low dilution rate applied during stratified periods, net population growth can occur.

Use, in the model, of a single set of rate constants for N remineralization, AO, and NO (*SI Appendix*, Table S4) was sufficient to reproduce the overall seasonal trends in DIN and *amoA* copies observed at 60 m from 2014 to 2017 (Fig. 3). Much of the observed inter- and intra-annual variability was resolved by this simple modeling approach, including the delayed nitrate production observed in 2014 (preintrusion) and 2015 as well as the immediate nitrate increases observed following 2015/16 winter mixing and the intrusion events in 2014 and 2016 (Fig. 3). A Q_{10}-type temperature dependence for the rate constants of AO, NO, and N remineralization

was required to represent the increased ammonium and nitrate production rates observed following intrusion events, which delivered warmer water (Fig. 1*B* and *SI Appendix*, Table S4 and *SI Discussion* S2). Some observations, such as the decrease in amoA-A1 abundance and the stop of nitrate accumulation in November 2016 despite ~6 μmol · kg_{sw}^{-1} ammonium still being present (Fig. 3 *B* and *C*) were not captured by the model. These mismatches are discussed in *SI Appendix*, *SI Discussion* S3.

Variability in Modeled Nitrification Rates Was Caused Mainly by the Dilution of Nitrifier Biomass by Physical Mixing. The modeled representation of AOO population density approximated the observed time series of amoA-A1 abundance (Fig. 3). After the long and intense winter mixing period of 2015 (Events M15 and PM15, Fig. 3*A*), which reduced the nitrifier population to very low levels (Fig. 2*C*), the modeled AO rate took several months to increase substantially (Fig. 3*D*) despite the presence of >5 μmol · kg_{sw}^{-1} ammonium during this period of delayed nitrification. In 2016, when shorter and less intense winter mixing resulted in less dilution of the nitrifier population, nitrification rates increased immediately after mixing ceased.

Experiments with the model were consistent with the observation that dilution of the AOO population during winter delayed nitrification: manipulation of the diluting effect of 2015 winter mixing on *amoA* gene copy numbers, while holding its effect on all other parameters constant, resulted in extended (increased influence of mixing on nitrifiers) or shortened (decreased influence) delay in both nitrifier growth and nitrate production (Fig. 4).

Results from a statistical evaluation of physical and geochemical parameters from the full-length BB time series (>10 y; *SI Appendix*, Tables S1 and S5 and *SI Discussion* S4) were also consistent with a role of winter mixing in delaying nitrification. Spiciness during the years 2014 to 2017 was lowest in March of 2015 (Event M15, Fig. 2*A*). Using data from the full-length time series, we observed that the magnitude of the annual spiciness minimum during winter (January through April) as well as the annual average oxygen concentration correlated with both the annual average nitrate concentration and the annual average value of the nitrate/ammonium ratio (*SI Appendix*, Table S5). The minimum spiciness and annual average oxygen concentration parameters may represent empirical indices of winter mixing intensity (minimum spiciness) and mixing intensity in general (average oxygen) so that these correlations are consistent with an overall negative effect of mixing on nitrification in BB.

Nitrite Accumulation as Another Consequence of Nitrifier Biomass Dilution. The model reproduced the nitrite peaks observed in September/October 2015 and 2017 (Fig. 3*B*). They appeared when modeled *amoA* exceeded *nxr* (the modeled functional gene for NO) during periods of regrowth following dilution of these populations (Fig. 3 *B* and *C*). This implies that nitrite accumulated due to decoupled regrowth of the two nitrifier populations after their dilution. Experiments with the model additionally demonstrated that increased dilution of nitrifier populations by mixing could have increased (and delayed) the accumulation of nitrite (Fig. 4). An additional influence of beta-AOB suggested by the observed coincidence of beta-AOB maxima with the 2015 and 2017 nitrite maxima (Fig. 2*D*) will be discussed below.

Discussion

Our analyses of the time series revealed that winter mixing controls nitrate production via its effect on nitrifier biomass and diversity (Fig. 2 and Table 1). During winter, surface water cooling drives convective mixing, which mixes the bottom waters with nitrifier-depleted near-surface water (*SI Appendix*, Fig. S5). The estuarine circulation and tidal exchange with offshore waters in the near-surface layers can then remove the nitrifiers from BB (37–39). Colder winters with stronger mixing were associated with stronger nitrifier biomass dilution that delayed nitrification by

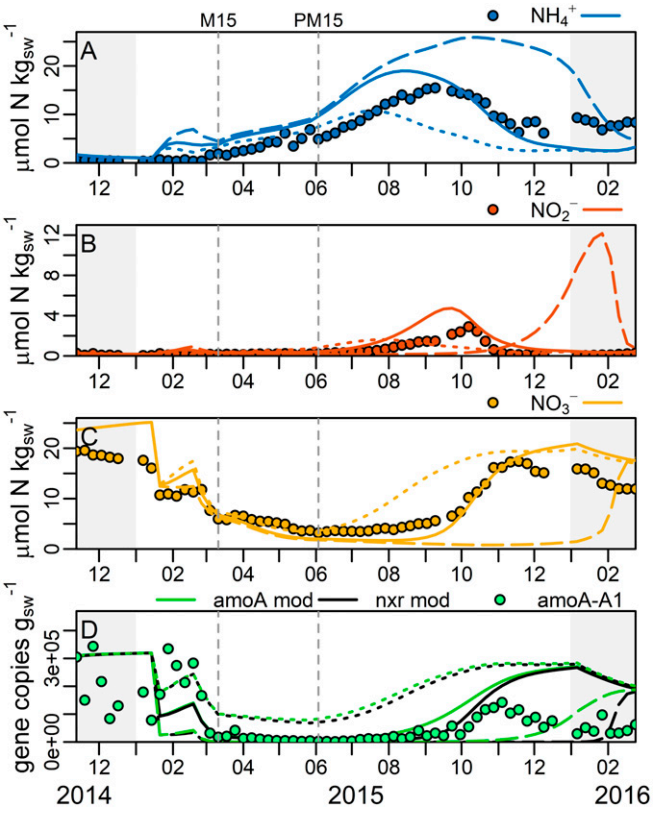

Fig. 4. Observations and model output as in Fig. 3 but focused on the year 2015 and showing the output from experimental model runs for which the effect of winter mixing on amoA and nxr was manipulated during winter mixing of 2015 (January 14th through May 27th). For this manipulation, the diluting effect of mixing on the nitrifier marker gene populations was multiplied by 2 (dashed lines) or divided by 2 (dotted lines) compared to the standard model (solid lines). (*A*) Ammonium concentrations; (*B*) nitrite concentrations; (*C*) nitrate concentrations; and (*D*) nxr (modeled only) and amoA concentrations. Event numbers ("M", "I", "PM", and "MDI") as in Fig. 1.

weeks to months and caused transient nitrite accumulation coinciding with beta-AOB growth (Fig. 2). The role of mixing is corroborated by statistical analyses of the long-term time series (*SI Appendix*, Tables S5 and S6 and *SI Discussion* S4). Additionally, a simple mechanistic model of microbial growth was able to reproduce observed interannual differences in nitrifier regrowth and the timing of nitrate accumulation based on variations in mixing intensity (Figs. 3 and 4).

On this basis, we propose a mechanism by which mixing dilutes nitrifier biomass, leading to both delay and decoupling of nitrification due to delays in nitrifier regrowth. This mechanism adds to a variety of environmental factors including light, copper, and temperature, which are known to potentially inhibit, limit, or decouple nitrification (20, 25, 48–51). As observed, ammonium that accumulated during periods of AO delay can eventually fuel fast AOO growth. Temporarily, this can outpace the regrowth of the NOB, which require time to adjust their population size once increased amounts of nitrite become available (Fig. 4). The resulting high AO rates temporarily exceed NO rates, which drives nitrite accumulation. As discussed in the following section, an additional effect of mixing on nitrifier community composition favored beta-AOB in their competition with AOA, which enhanced the nitrite accumulation.

Transient Beta-AOB Growth Is Associated with Nitrite Accumulation and Suggests Mixing-Induced Shifts in Ammonia Oxidizer Dominance. *Nitrosopumilus*-like *Thaumarchaeota* (AOA) of the amoA-A1 phylotype were consistently present in BB bottom water and were

overall the most abundant ammonia oxidizers during the 4 y period. However, we also observed short-lived peaks in beta-AOB–affiliated ASVs that coincided with the largest nitrite accumulations and were followed by steep increases of nitrate (Fig. 2 *B* and *D*). These AOB peaks appeared when high ammonium concentration coincided with strong dilution of the nitrifier community in 2015 and after the middepth intrusion of July 2017, which suggests that opportunistic, fast-growing AOB temporarily outcompeted slower-growing AOA and were involved in creating the relatively large (>1 μmol · kg_{sw}^{-1}) nitrite accumulations. As these AOB eventually became substrate limited by depleting ammonium to levels below their K_m, the AOA population re-established its dominance (Fig. 2 *C* and *D*). In 2016, relatively weak winter mixing allowed the resident AOA population to persist through the winter so that it was ready to utilize ammonium as it became available following the onset of stratification (Fig. 2 *A*–*C*). Even when ammonium accumulated to high concentrations later that year, the AOA were established in a stable environment, which allowed them to outcompete AOB. Hence, we suggest that mixing created temporary niches for the beta-AOB, which have higher V_{max} and K_m compared to AOA (6–11). The fast enzyme kinetics of beta-AOB likely enhanced nitrite accumulation by promoting decoupling from NOB growth and further translated into steep increases of nitrate once the NOB population was large enough to decrease the initially accumulated nitrite.

We note that the slow and steady nitrate increase of the 2016 stratified period, when AOB played a negligible role, was overestimated by the model, whereas the steep nitrate increase in September/October 2017, which was associated with the highest abundance of AOB-affiliated ASVs (Fig. 2 *C* and *D*), was reproduced more closely (Fig. 3*C*). This suggests that the fixed set of rate constants employed in the model are more representative of faster "AOB-type" AO (2015 and 2017) than slower "AOA-type" AO (2014 and 2016). This may also explain the "false" nitrite peaks generated by the model during the AOA-dominated years 2014 and 2016 (Fig. 3*B*).

A model version adjusted to "AOA-type" AO would therefore be expected to improve the fit to the observations made in 2016. Indeed, use of a different AO parameterization in an otherwise identical model better represented the absence of strong nitrite accumulation and the steady nitrate increase observed in 2016 but strongly overestimated the delay in nitrate accumulation in 2015 and 2017 (*SI Appendix*, Fig. S7). For the purpose of this study, the simple model with a single AOO population (Fig. 3) was valuable in demonstrating that the interannual differences in nitrite and nitrate accumulation were independent of variable AO kinetics. Yet, the model adjusted to 2016 observations (*SI Appendix*, Fig. S7) provided insights on a more granular level and showed that slower AOA kinetics could better simulate the conditions of 2016 (steady nitrate increase and absence of even a small nitrite maximum). In the future, a more complex model with at least two kinetically distinct AOO populations would be required to further explore the competition based on the kinetic differences between AOB and AOA. The observations presented here demonstrate how mixing can affect not only the biomass of nitrifiers but also their community composition, both having consequences for the transformation of N species. This, in turn, suggests that explicit modeling of nitrifier biomass and its diversity is important for understanding N cycling in dynamic coastal systems and projecting its response to variable climate forcing.

Control by Physical Mixing Explains Seasonal Changes in AO Rates. Similar ranges and variability in AO rates as described here were observed in BB bottom water by Punshon and Moore (31), who measured AO rates using isotopic labeling experiments throughout 2002 but did not have supporting data describing the nitrifier community. Notably, they found no correlation of AO rates with either temperature or ammonium concentration but instead an association of low rates with winter mixing, which led them to speculate about an influence of nitrifier biomass on AO rates.

Here, we are able to show that this lack of correlation as well as variable AO rates are indeed consequences of variable nitrifier biomass, which masks the effect of ammonium and temperature on AO rates. Our model, which includes nitrifier biomass, temperature, and ammonium concentration on AO rates (*SI Appendix*, Table S3), was able to reproduce the trends observed in BB bottom water during 2002 following adjustment of mixing and surface boundary conditions to reflect the conditions of that year (*SI Appendix*, Fig. S8). That is, using model parameterizations that had been tuned to represent the 2014-through-2017 time series (Fig. 3), it was possible to reproduce the independently collected nitrate and ammonium concentration data and AO rates measured in 2002 (*SI Appendix*, Fig. S8). This suggests that dilution of ammonia oxidizer biomass by winter mixing was the reason for the low rates of AO measured in March 2002 (31).

An alternative hypothesis to biomass dilution for an effect of mixing on AO rates could be "cold shock" associated with a sudden decrease in temperature upon the initiation of convective mixing. Cold shock might inhibit nitrification to an extent greater than the Q_{10} temperature dependency included in the model. However, laboratory studies suggest that such effects are relatively small and short lived (order of a few days) in nitrifiers shocked by a sudden 10 °C temperature decrease (52). By contrast, the largest observed temperature decrease in BB bottom water between 2014 and 2017 was 3.4 °C · $week^{-1}$ (in February 2015).

Broader Significance of Mixing-Induced Dilution and Shifting of Nitrifier Communities. Any water column subject to intermittent stratification may, in principle, be susceptible to the identified control of mixing on nitrification. If water supplied by mixing or advection is relatively poor in viable nitrifier biomass but contains ammonium or organic N, ammonium and nitrite may consequently accumulate due to delayed nitrification and associated temporal decoupling of nitrification. This could apply to subsurface waters of seasonally mixed lakes where climatic variations can affect the extent of spring mixing (53) as well as fjord-like basins and estuaries similar to BB with seasonal stratification–mixing cycles and/or irregular intrusion events (22, 35, 54). The mechanism might even operate in shelf ecosystems subject to seasonal blooms and sinking of organic matter, periodic upwelling, or seasonal changes in shelf–slope exchange (15, 55, 56).

Hence, similar mixing-related control mechanisms on nitrification may be widespread, but high-frequency time series of long duration that include microbiological markers to trace biomass variations may be required to recognize and elucidate their global distribution. The sparsity of such time series datasets, especially those with high temporal resolution, might explain why such a mechanism has not been described previously.

There are, however, some indications in the literature for its occurrence. For example, higher *Thaumarchaeota* numbers were observed in near-surface waters of Monterey Bay during stratification in fall compared to relatively unstratified waters in spring (33). Hollibaugh et al. (57) made similar observations using seasonal sampling in coastal near-surface waters off Georgia: the highest copy numbers of thaumarchaeal *amoA* and 16S rRNA genes were found at the end of the stratified period, while much lower numbers were found earlier in the stratified period and prior to the onset of stratification. A follow-up study on the same system suggested that accelerated growth of AOA under high summer temperatures might have been responsible for the decoupling of nitrification and nitrite accumulation (20). However, the observed increase of AOA during the stratified period are also consistent with the mechanism presented here, whereby physical mixing dilutes the nitrifier community, causing nitrite peaks upon AOA regrowth.

Seasonal variations in nitrification and nitrifier biomass as well as transient nitrite accumulation have been observed in many other marine coastal and shelf systems, and the causal mechanisms are often poorly understood (20, 21, 33, 55, 57, 58). Schaefer and Hollibaugh (20) suggested that high temperature may decouple nitrification by promoting rapid AOO growth. Decoupling by rapid AOO growth may also underlie observations of nitrification decoupling associated with sudden availability of ammonium (35, 46). The mechanism involving physical dilution described here relies on a similar principle to decouple nitrification by eventual fast AOO growth (following delayed AOO regrowth), leading to AO > NO and nitrite accumulation (Fig. 4 *B* and *D*). This suggests that, rather than NOB inhibition or limitation, AOO growth variations that cannot be immediately matched by NOB growth may be a common driver of transient nitrite accumulation in many aquatic systems.

Nitrifier Biomass Dilution as a Link between Climate, Nitrification, and Phytoplankton Ecology. Our study reveals how mixing can affect functional microbial communities with biogeochemical consequences on seasonal and interannual timescales. The timing of nitrification in BB bottom water varies with the degree of "washout" (via mixing) of nitrifier populations which develop during the previous year. This demonstrates an interannual "memory" of biogeochemical conditions in this coastal ecosystem that can be conveyed by the over-wintering of microbial communities but that can also be erased by periods of strong mixing. Effects of mixing on microbial biomass have been described previously (28, 30), but our analyses also demonstrate how physical mixing can lead to alterations in functional microbial community composition by creating conditions under which AOB can outcompete AOA.

The variable nitrifier biomass dilution might therefore control the speciation of DIN in subsurface waters. This can influence phytoplankton growth upon resupply of subsurface DIN by destratification or upward transport mechanisms to sunlit waters (17). Within BB, for example, intrusion-driven upwelling could affect phytoplankton ecology by delivering DIN to the euphotic zone, which tends to be N limited (*SI Appendix*, Fig. S9) and low in ammonium and nitrate during summer (36). The variable speciation of supplied DIN can impact phytoplankton ecology and the health of aquatic ecosystems. For example, a high share of ammonium in DIN supply has been linked to lower primary productivity and selection against diatoms and toward smaller algal species with higher potential to form harmful algae blooms (2–4).

The link between mixing and nitrification can control not only the speciation but also the quantity of fixed N available to primary producers, since oxidized forms of nitrogen are the substrate for denitrification. Low-oxygen coastal environments are responsible for a significant fraction of global N removal (59, 60). Therefore, alterations in the balance between fixed N retention and removal in such systems due to variable nitrification may have larger-scale consequences for N cycling.

Moreover, all these effects are linked to weather and climate, since atmospheric forcing plays an important role for stratification–mixing patterns of ocean waters (61). For example, infrequent deep water renewal events in a coastal basin have been linked to variations in freshwater run-off and other atmospherically controlled variables (54). In BB, winter mixing is largely driven by heat loss to the atmosphere (32, 39). Since strong winter mixing can delay nitrification, air temperatures and heat loss during winter can influence the timing and extent of nitrification over the remainder of the year. Our findings show how weather and climate variability can drive variations in DIN speciation with biogeochemical implications for phytoplankton ecology and fixed N budgets. Previous examples of climate–ecosystem connections involving nitrogen speciation have focused on variations in external nitrogen supply to coastal bays, such as the relative supply of inorganic versus organic forms of N (5). Here, however, the link is made via physical controls on microbial community composition.

For Atlantic Canada, as for many other temperate regions, the increase in winter temperatures and changes in storm patterns observed over the past decades are projected to continue as a consequence of climate change (62, 63). It is tempting to speculate that climate change will result in reduced wintertime convective mixing in BB as a result of strengthened haline stratification in winter due to increased freshwater input (increased precipitation or decreased freshwater retention in snow cover) and/or milder winter temperatures (reduced heat loss). However, climate-related changes of mixing intensity in other coastal systems may be very different. Assuming a scenario of decreased winter mixing and notwithstanding any secondary effects such as lower oxygen concentration due to decreased ventilation, our findings would suggest a strengthening of the interannual memory of the system and therefore less delay in nitrate production.

The high (weekly) resolution of the BB time series was an essential prerequisite to identify and understand the complex patterns of nitrifier diversity and N speciation and their connection to physical forcing. This emphasizes the importance of multiparameter, high-frequency oceanographic time series in combination with biogeochemical models for elucidating the complicated interactions between microbial communities and the physical conditions they are subjected to. Such approaches are needed to understand and project the impacts of variable forcing and climate change on microbial communities and biogeochemical processes in dynamic coastal environments.

Materials and Methods

Bedford Basin Study Site, Sampling, and Time Series Context. Descriptions of the study site, the long-term time series context, sampling procedures, and the source of atmospheric data are detailed in *SI Appendix, SI Materials and Methods*.

Analysis of Bulk Nutrient, Particulate, and Chlorophyll *a* Concentrations. Nutrients, particulates, and chlorophyll *a* were analyzed by standard methodology, as detailed in *SI Appendix, SI Materials and Methods*.

Numerical Modeling. A time-resolved box model was used to simulate annual N cycling in the bottom water of BB and investigate possible mechanisms for temporal decoupling of N remineralization, AO and NO (*SI Appendix*, Fig. S6). The use of a box model was motivated by a lack of spatial resolution in our data set and the philosophy of not making the model more complicated than the resolution of the data we are seeking to understand. The model equations (*SI Appendix*, Table S2) compute the change in state variable concentration (dC/dt) with time. These include chemical concentrations (O_2, NH_3/NH_4^+, NO_2^-, and NO_3^-), and two microbial populations, represented by the marker genes for ammonia (*amoA*) and nitrite oxidation (*nxr*). A complete list of differential equations, reactions, and rate parameters are presented in *SI Appendix*, Tables S2–S4. The initial remineralization reaction was forced by weekly particulate organic carbon (POC) data from 60 m and accounted for seasonal variability in remineralization (e.g., the spring bloom), which was not explicitly represented in the model. Remineralization consumes POC and O_2, producing NH_3/NH_4^+ according to the Redfield ratio (*SI Appendix*, Table S3). Nitrification was modeled as a two-step process: AO ($NH_3/NH_4^+ \rightarrow NO_2^-$) facilitated by ammonia oxidizers (*amoA*) and NO ($NO_2^- \rightarrow NO_3^-$) facilitated by nitrite oxidizers (*nxr*), both also consuming O_2. A Q_{10} formulation was used to represent the influence of temperature on the rate constants for remineralization and nitrification (*SI Appendix*, Table S3). A loss term for NO_3^- (a first-order function of nitrate concentration, *SI Appendix*, Table S3) was included, representing the loss of NO_3^- to N assimilation by chemoautotrophs as well as denitrification, both in the sediment and potentially the anoxic microzones associated with particles (64). Empirically, it accounts for the fact that remineralization with Redfield stoichiometry over-predicts DIN concentrations in the latter half of each year when DIN:P ratios decline at 60 m in BB (*SI Appendix*, Fig. S9). A loss term for O_2 represents sediment uptake and was based on measured O_2 uptake by BB sediments (65).

The model assumes that the bottom water of BB is one stable box that only marginally interacts with the near-surface water (5 m) during the stratified period which prevails for most of the year. During mixing periods (winter/spring), the water column overturns, mixing the bottom water with near-surface water.

Additionally, short-lived, randomly timed intrusions introduce shelf-water into the bottom water. Mixing was implemented with the following mathematical relationship:

$$\left.\frac{\partial C_i}{\partial t}\right|_{mix} = \frac{1}{\tau} \times \left(C_i^{5m} - C_i\right), \quad [3]$$

where C_i is the concentration at 60 m of the state variable in question, C_i^{5m} is its concentration in the near-surface water (5 m), and τ is the exchange timescale of bottom water with near-surface water from within the basin or the Scotian Shelf. For the stratified period, this timescale was chosen based on the eddy diffusivity values from BB determined by Burt et al. (41) and a length scale from the depth of the sill to the bottom of basin (~50 m) according to the relation h^2/K_z. During the intrusion events, τ was decreased to a small value to recreate the sudden step-like O_2 concentration changes observed in our weekly time series. During winter, when convective cooling and storms homogenize the basin water, τ was decreased to reproduce the specifically observed increase in bottom water O_2 during this time. O_2 was used as tracer of mixing, because its nonconservative nature makes it a particularly sensitive tracer of active mixing. Since the surface was the only source of O_2 to the bottom water, active mixing at a rate exceeding O_2 consumption was needed to increase or maintain O_2 concentrations. Conservative tracers (e.g., salinity) once equalized between bottom and near-surface water can become insensitive to further mixing in the following weeks, whereas biological O_2 consumption quickly resets O_2 as a tracer sensitive to further mixing. It is assumed that the timeseries of weekly measurements at 5 m depth for O_2, NO_3^-, NO_2^-, and NH_3/NH_4^+ are representative of the near-surface water that is exchanged with the basin bottom water and are used as the top boundary condition. The concentrations of *amoA* and *nxr* were taken to be 0 in the near-surface water (*SI Appendix*, Fig. S5). Unlike the remaining intrusion and winter mixing events, the 2017 middepth intrusion was modeled as an exchange of 60 m water with a water mass representing BB middepth water (200 μmol O_2 kg_{sw}^{-1}, 12 μmol NH_4^+ kg_{sw}^{-1}, 5 μmol NO_3^- kg_{sw}^{-1}, 0 μmol NO_2^- kg_{sw}^{-1}, and 0 gene populations).

To constrain the kinetic parameters, the O_2 half-saturation constants for AO and NO were chosen from literature values (*SI Appendix*, Table S4). The rate constants for remineralization (*k.remin*), AO (*k.AO*), and NO (*k.NO*) were fit to the 4 y times series by minimizing the cost function:

$$\sum_j \sum_i \left(\frac{y_{ij}^{mod} - y_{ij}^{obs}}{\bar{y}_i}\right)^2, \quad [4]$$

where y_{ij}^{mod} and y_{ij}^{obs} are the modeled and observed concentrations of i (O_2, NO_3^-, NO_2^-, and NH_3/NH_4^+) at time , and $\bar{y}_i$ is the average concentration of each in the time series. The model was coded in the programing language R, using the package "deSolve" to solve differential equations (66) and the package "FME" for least-square fitting (67).

Microbial Cell Counts. Total microbial cells <35 μm were stained with SYBR Green I (Invitrogen) and quantified by flow cytometry, as detailed in *SI Appendix, SI Materials and Methods*.

DNA Extraction, 16S rRNA Amplicon Sequencing and Sequence Analysis. DNA extractions of 0.2 to 160 μm of fractionated seawater were completed as previously described (68), and amplicon sequencing of the V4 to V5 variable region of the16S rRNA gene of bacteria and archaea was conducted at the Integrated Microbiome Resource, Dalhousie University (ref. 69 and methodology therein). Illumina sequences of the 16S rRNA gene were processed using a QIIME 2–based workflow (70) as described in *SI Appendix, SI Materials and Methods*. Phylogenetic trees were built as described in *SI Appendix, SI Materials and Methods*.

qPCRs. Six oceanic archaeal phylotypes of the archaeal *amoA* gene (amoA-A1, -A2, -A3, -A4, -A5 and -A6) as defined by Sintes et al. (47) were quantified by qPCR. Details of the assays used to quantify the different phylotypes can be found in *SI Appendix, SI Materials and Methods* and Tables S7 and S8.

Data Availability. All data required to evaluate the conclusions of this study are included in the paper and/or the *SI Appendix*. Quantitative molecular, geochemical, and physical data as well as the model code have been deposited in PANGAEA (https://doi.pangaea.de/10.1594/PANGAEA.914705). Sequence data from this article can be found in the GenBank data library (https://www.ncbi.nlm.nih.gov/genbank/) under the accession numbers MT175443–MT175495. The subset of data produced by the Bedford Institute of Oceanography can additionally be accessed under this link: https://www.bio.gc.ca/science/monitoring-monitorage/bbmp-pobb/bbmp-pobb-en.php.

ACKNOWLEDGMENTS. This work was funded by the Canada Excellence Research Chair for Ocean Science and Technology. Additionally, S.H. was supported by a Nova Scotia Graduate Scholarship (NSGS) and a Killam Predoctoral Scholarship, B.M.R. by a Natural Sciences and Engineering Research Council of Canada (NSERC), Canada Graduate Scholarship – Doctoral award, S.R. by an NSGS and by the Transatlantic Graduate Research School, J.L. and J.T. by the Ocean Frontier Institute and an NSERC Grant to J.L., and C.K.A. by an NSERC Discovery Grant. We thank Anna Haverstock, Elizabeth Kerrigan, Claire Normandeau, and their coworkers for laboratory and field work. Bill Li, Andrew Cogswell, and the Bedford Institute of Oceanography deserve credit for starting and maintaining the time series. Ciara Willis, Jackie Zorz, Jenni-Marie Ratten, and Ian Luddington helped with the collection of the DNA samples. The Coastal Environmental Observation Technology and Research team led by Richard Davis and supported by the Marine Environmental Observation, Prediction and Response Network (MEOPAR) provided valuable data, and Dariia Atamanchuk and Kate Patterson helped to make them available. Finally, we thank Daniel Kelley, Michael Dowd, and Carolyn Buchwald for helpful discussions as well as four anonymous reviewers for valuable ideas to improve the manuscript.

1. J. Peñuelas *et al.*, Human-induced nitrogen-phosphorus imbalances alter natural and managed ecosystems across the globe. *Nat. Commun.* **4**, 2934 (2013).
2. P. M. Glibert *et al.*, Pluses and minuses of ammonium and nitrate uptake and assimilation by phytoplankton and implications for productivity and community composition, with emphasis on nitrogen-enriched conditions. *Limnol. Oceanogr.* **61**, 165–197 (2016).
3. K. Yoshiyama, J. H. Sharp, Phytoplankton response to nutrient enrichment in an urbanized estuary: Apparent inhibition of primary production by overeutrophication. *Limnol. Oceanogr.* **51**, 424–434 (2006).
4. R. B. Domingues, A. B. Barbosa, U. Sommer, H. M. Galvão, Ammonium, nitrate and phytoplankton interactions in a freshwater tidal estuarine zone: Potential effects of cultural eutrophication. *Aquat. Sci.* **73**, 331–343 (2011).
5. J. LaRoche *et al.*, Brown tide blooms in Long Island's coastal waters linked to interannual variability in groundwater flow. *Glob. Change Biol.* **3**, 397–410 (1997).
6. I. Suzuki, U. Dular, S. C. Kwok, Ammonia or ammonium ion as substrate for oxidation by *Nitrosomonas europaea* cells and extracts. *J. Bacteriol.* **120**, 556–558 (1974).
7. A. Bollmann, I. Schmidt, A. M. Saunders, M. H. Nicolaisen, Influence of starvation on potential ammonia-oxidizing activity and *amoA* mRNA levels of *Nitrosospira briensis*. *Appl. Environ. Microbiol.* **71**, 1276–1282 (2005).
8. B. B. Ward, Kinetic studies on ammonia and methane oxidation by *Nitrosococcus oceanus*. *Arch. Microbiol.* **147**, 126–133 (1987).
9. W. Martens-Habbena, P. M. Berube, H. Urakawa, J. R. de la Torre, D. A. Stahl, Ammonia oxidation kinetics determine niche separation of nitrifying Archaea and bacteria. *Nature* **461**, 976–979 (2009).
10. R. E. A. Horak *et al.*, Ammonia oxidation kinetics and temperature sensitivity of a natural marine community dominated by Archaea. *ISME J.* **7**, 2023–2033 (2013).
11. X. Peng *et al.*, Revisiting nitrification in the Eastern Tropical South Pacific : A focus on controls. *J. Geophys. Res. Oceans* **121**, 1667–1684 (2016).
12. H. Daims *et al.*, Complete nitrification by *Nitrospira* bacteria. *Nature* **528**, 504–509 (2015).
13. M. A. H. J. van Kessel *et al.*, Complete nitrification by a single microorganism. *Nature* **528**, 555–559 (2015).
14. F. Xia *et al.*, Ubiquity and diversity of complete ammonia oxidizers (comammox). *Appl. Environ. Microbiol.* **84**, e01390–e18 (2018).
15. A. E. Santoro *et al.*, Measurements of nitrite production in and around the primary nitrite maximum in the central California current. *Biogeosciences* **10**, 7395–7410 (2013).
16. A. Yool, A. P. Martin, C. Fernández, D. R. Clark, The significance of nitrification for oceanic new production. *Nature* **447**, 999–1002 (2007).
17. K. S. Johnson, S. C. Riser, D. M. Karl, Nitrate supply from deep to near-surface waters of the North Pacific subtropical gyre. *Nature* **465**, 1062–1065 (2010).
18. M. W. Lomas, F. Lipschultz, Forming the primary nitrite maximum: Nitrifiers or phytoplankton? *Limnol. Oceanogr.* **51**, 2453–2467 (2006).
19. E. M. Heiss, R. W. Fulweiler, Coastal water column ammonium and nitrite oxidation are decoupled in summer. *Estuar. Coast. Shelf Sci.* **178**, 110–119 (2016).
20. S. C. Schaefer, J. T. Hollibaugh, Temperature decouples ammonium and nitrite oxidation in coastal waters. *Environ. Sci. Technol.* **51**, 3157–3164 (2017).
21. S. M. Laperriere, N. J. Nidzieko, R. J. Fox, A. W. Fisher, A. E. Santoro, Observations of variable ammonia oxidation and nitrous oxide flux in a eutrophic estuary. *Estuaries Coasts* **42**, 33–44 (2019).
22. S. G. Horrigan *et al.*, Nitrogenous nutrient transformations in the spring and fall in the Chesapeake Bay. *Estuar. Coast. Shelf Sci.* **30**, 369–391 (1990).
23. J. M. Beman, R. Sachdeva, J. A. Fuhrman, Population ecology of nitrifying *archaea* and *bacteria* in the Southern California Bight. *Environ. Microbiol.* **12**, 1282–1292 (2010).
24. K. Kitzinger *et al.*, Single cell analyses reveal contrasting life strategies of the two main nitrifiers in the ocean. *Nat. Commun.* **11**, 767 (2020).
25. S. Philips, H. Laanbroek, W. Verstraete, Origin, causes and effects of increased nitrite concentrations in aquatic environments. *Rev Environ* **1**, 115–141 (2002).
26. L. A. Bristow *et al.*, Biogeochemical and metagenomic analysis of nitrite accumulation in the Gulf of Mexico hypoxic zone. *Limnol. Oceanogr.* **60**, 1733–1750 (2015).

27. S. Dutkiewicz, M. Follows, J. Marshall, W. W. Gregg, Interannual variability of phytoplankton abundances in the North Atlantic. *Deep Res Part II Top Stud Oceanogr* **48**, 2323–2344 (2001).
28. M. J. Behrenfeld, Abandoning sverdrup's critical depth hypothesis on phytoplankton blooms. *Ecology* **91**, 977–989 (2010).
29. J. J. McCarthy, W. Kaplan, J. L. Nevins, Chesapeake Bay nutrient and plankton dynamics. 2. Sources and sinks of nitrite. *Limnol. Oceanogr.* **29**, 84–98 (1984).
30. E. J. Zakem *et al*., Ecological control of nitrite in the upper ocean. *Nat. Commun.* **9**, 1206 (2018).
31. S. Punshon, R. M. Moore, Nitrous oxide production and consumption in a eutrophic coastal embayment. *Mar. Chem.* **91**, 37–51 (2004).
32. W. K. W. Li, W. G. Harrison, Propagation of an atmospheric climate signal to phytoplankton in a small marine basin. *Limnol. Oceanogr.* **53**, 1734–1745 (2008).
33. J. C. Robidart *et al*., Seasonal *Synechococcus* and *Thaumarchaeal* population dynamics examined with high resolution with remote *in situ* instrumentation. *ISME J.* **6**, 513–523 (2012).
34. H. El-Swais, K. A. Dunn, J. P. Bielawski, W. K. W. Li, D. A. Walsh, Seasonal assemblages and short-lived blooms in coastal north-west Atlantic Ocean bacterioplankton. *Environ. Microbiol.* **17**, 3642–3661 (2015).
35. X. Ma, S. T. Lennartz, H. W. Bange, A multi-year observation of nitrous oxide at the Boknis Eck time series station in the Eckernförde bay (southwestern Baltic sea). *Biogeosciences* **16**, 4097–4111 (2019).
36. W. K. W. Li, The state of phytoplankton and bacterioplankton at the compass Buoy station: Bedford basin monitoring program 1992-2013. *Can Tech Rep Hydrogr Ocean Sci* **304**, 1–122 (2014).
37. B. Petrie, P. Yeats, Simple models of the circulation, dissolved metals, suspended solids and nutrients in Halifax Harbour. *Water Qual. Res. J. Canada* **25**, 325–349 (1990).
38. G. Fader, R. Miller, Surficial geology, Halifax Harbour, Nova Scotia. *Geol Surv Canada Bull* **590**, 1–165 (2008).
39. S. Shan, J. Sheng, K. R. Thompson, D. A. Greenberg, Simulating the three-dimensional circulation and hydrography of Halifax Harbour using a multi-nested coastal ocean circulation model. *Ocean Dyn.* **61**, 951–976 (2011).
40. T. Platt, A. Prakash, B. Irwin, Phytoplankton nutrients and flushing of inlets on the coast of Nova Scotia. *Nat. Can.* **99**, 253–261 (1972).
41. W. J. Burt, H. Thomas, K. Fennel, E. Horne, Sediment-water column fluxes of carbon, oxygen and nutrients in Bedford Basin, Nova Scotia, inferred from ^{224}Ra measurements. *Biogeosciences* **10**, 53–66 (2013).
42. S. Taguchi, T. Platt, Assimilation of $^{14}CO_2$ in the dark compared to phytoplankton production in a small coastal inlet. *Estuar. Coast. Mar. Sci.* **5**, 679–684 (1977).
43. A. A. Georges, H. El-Swais, S. E. Craig, W. K. Li, D. A. Walsh, Metaproteomic analysis of a winter to spring succession in coastal northwest Atlantic Ocean microbial plankton. *ISME J.* **8**, 1301–1313 (2014).
44. Q. Shi, D. Wallace, A 3-year time series of volatile organic iodocarbons in Bedford Basin, Nova Scotia: A northwestern Atlantic fjord. *Ocean Sci.* **14**, 1385–1403 (2018).
45. P. Flament, A state variable for characterizing water masses and their diffusive stability: Spiciness. *Prog. Oceanogr.* **54**, 493–501 (2002).
46. A. Pitcher, C. Wuchter, K. Siedenberg, S. Schouten, J. S. Sinninghe Damsté, Crenarchaeol tracks winter blooms of ammonia-oxidizing Thaumarchaeota in the coastal North Sea. *Limnol. Oceanogr.* **56**, 2308–2318 (2011).
47. E. Sintes, D. De Corte, E. Haberleitner, G. J. Herndl, Geographic distribution of archaeal ammonia oxidizing Ecotypes in the Atlantic Ocean. *Front. Microbiol.* **7**, 77 (2016).
48. S. B. Joye, J. T. Hollibaugh, Influence of sulfide inhibition of nitrification on nitrogen regeneration in sediments. *Science* **270**, 623–625 (1995).
49. J. Groeneweg, B. Sellner, W. Tappe, Ammonia oxidation in Nitrosomonas at NH_3 concentrations near K_m: Effects of pH and temperature. *Water Res.* **28**, 2561–2566 (1994).
50. S. N. Merbt *et al*., Differential photoinhibition of bacterial and archaeal ammonia oxidation. *FEMS Microbiol. Lett.* **327**, 41–46 (2012).
51. S. A. Amin *et al*., Copper requirements of the ammonia-oxidizing archaeon *Nitrosopumilus maritimus* SCM1 and implications for nitrification in the marine environment. *Limnol. Oceanogr.* **58**, 2037–2045 (2013).
52. J. H. Hwang, J. A. Oleszkiewicz, Effect of cold-temperature shock on nitrification. *Water Environ. Res.* **79**, 964–968 (2007).
53. N. Salmaso, Effects of climatic fluctuations and vertical mixing on the interannual trophic variability of Lake Garda, Italy. *Limnol. Oceanogr.* **50**, 553–565 (2005).
54. S. Kelly, E. Eyto, M. Dillane, R. Poole, M. White, Characterizing ventilation events in an anoxic coastal basin: Observed dynamics and the role of climatic drivers. *Limnol. Oceanogr.* **9999**, 1–23 (2020).
55. C. W. Mordy *et al*., Temporary uncoupling of the marine nitrogen cycle: Accumulation of nitrite on the Bering Sea shelf. *Mar. Chem.* **121**, 157–166 (2010).
56. M. E. White, P. A. Rafter, B. M. Stephens, S. D. Wankel, L. I. Aluwihare, Recent increases in water column denitrification in the seasonally suboxic bottom waters of the Santa Barbara basin. *Geophys. Res. Lett.* **46**, 6786–6795 (2019).
57. J. T. Hollibaugh *et al*., Seasonal variation in the metatranscriptomes of a Thaumarchaeota population from SE USA coastal waters. *ISME J.* **8**, 685–698 (2014).
58. S. G. Horrigan, A. L. Springer, Oceanic and estuarine ammonium oxidation: Effects of light. *Limnol. Oceanogr.* **35**, 479–482 (1990).
59. M. Voss *et al*., The marine nitrogen cycle: Recent discoveries, uncertainties and the potential relevance of climate change. *Philos. Trans. R. Soc. Lond. B Biol. Sci.* **368**, 20130121 (2013).
60. S. Sokoll *et al*., Extensive nitrogen loss from permeable sediments off North-West Africa. *J. Geophys. Res. Biogeosci.* **121**, 1144–1157 (2016).
61. A. Capotondi, M. A. Alexander, N. A. Bond, E. N. Curchitser, J. D. Scott, Enhanced upper ocean stratification with climate change in the CMIP3 models. *J. Geophys. Res. Ocean* **117** (2012).
62. X. Zhang *et al*., "Changes in temperature and precipitation across Canada" in *Canada's Changing Climate Report*, E. Bush, D. Lemmen, Eds. (Government of Canada, 2019), pp. 112–193.
63. B. J. W. Greenan *et al*., "Changes in oceans surrounding Canada" in *Canada's Changing Climate Report*, E. Bush, D. Lemmen, Eds. (Government of Canada, 2019), pp. 343–423.
64. D. Bianchi, T. S. Weber, R. Kiko, C. Deutsch, Global niche of marine anaerobic metabolisms expanded by particle microenvironments. *Nat. Geosci.* **11**, 263–268 (2018).
65. B. T. Hargrave, Seasonal changes in oxygen uptake by settled particulate matter and sediments in a marine bay. *J. Fish. Res. Board Can.* **35**, 1621–1628 (1978).
66. K. Soetaert, T. Petzoldt, R. W. Setzer, Solving differential equations in R: Package deSolve. *J. Stat. Softw.* **33**, 1–25 (2010).
67. K. Soetaert, T. Petzoldt, Inverse modelling, sensitivity and Monte Carlo analysis in R using package FME. *J. Stat. Softw.* **33**, 1–28 (2010).
68. S. Haas, D. K. Desai, J. LaRoche, R. Pawlowicz, D. W. R. Wallace, Geomicrobiology of the carbon, nitrogen and sulphur cycles in Powell Lake: A permanently stratified water column containing ancient seawater. *Environ. Microbiol.* **21**, 3927–3952 (2019).
69. A. M. Comeau, G. M. Douglas, M. G. I. Langille, Microbiome helper: A custom and streamlined workflow for microbiome research. *mSystems* **2**, e00127–e16 (2017).
70. E. Bolyen *et al*., Reproducible, interactive, scalable and extensible microbiome data science using QIIME 2. *Nat. Biotechnol.* **37**, 852–857 (2019).